Journal of Petroleum Science and Engineering 94–95 (2012) 28–39

Contents lists available at SciVerse ScienceDirect

Journal of Petroleum Science and Engineering

journal homepage: www.elsevier.com/locate/petrol

Effect of normally distributed porosities on dissolution pattern in carbonate acidizing

Ming Liu*, Shicheng Zhang, Jianye Mou

MOE Key Laboratory of Petroleum Engineering, China University of Petroleum, Beijing, China

ARTICLE INFO

Article history:
Received 11 October 2011
Accepted 2 June 2012
Available online 19 June 2012

Keywords:
Heterogeneity
Carbonate acidizing
Wormhole propagation
Skin factor

ABSTRACT

In carbonate acidizing, acid dissolves rock to create a high permeability channel called wormhole. One of the main factors to influence the formation of wormhole is the heterogeneity of porous medium. In former literature, uniformly distributed porosity fields were considered which are not in accord with the real distribution of porosities in rocks. In this paper, we use a normal distribution method to generate porosities. The comparison of the two methods shows that the pore volume to breakthrough for the normal distribution method is less than that for the uniform distribution method. Due to the characteristics of normal law, correlation length and standard deviation which characterize heterogeneity are introduced. The correlation in the radial or circumferential direction among girds has an effect on wormholing. Wormhole tends to propagate away from the radial direction to make itself thicker due to the big correlation length in the circumferential direction. The number of wormholes is increased and the wormholes become thinner because of big correlation length in the radial direction. The total acid injection volume decreases with the increase of initial porosity. A critical value for standard deviation exists, below which the pore volume to breakthrough is insensitive, above which the pore volume to breakthrough decreases sharply. The increase of perforation length decreases the pore volume to breakthrough whether there is acid leakoff along the perforation or not. The sharp decline of pressure at the end for the face dissolution pattern is due to the faster propagation velocity for the spent acid front than that for the reaction front and the short distance between them. Continuous vugs change the wormhole propagation path and decrease the injection volume. Finally, an apparent skin factor model is developed to study the performance of wormholing. Before the breakthrough of the damage zone, the sharply decreased skin factor indicates huge improvement, after the breakthrough, the skin factor decreases slowly. Wormhole length and time follow a power–law relationship.

1. Introduction

In carbonate reservoirs, acidizing is one of the most successful methods to improve the damage near the wellbore which may be caused by fines migration or drilling. Hydrochloric acid is the most commonly used acid to dissolve the minerals present in formation, which can create a high permeability channel so that the hydrocarbons bypass the damage zone to flow into the wellbore.

Experimental and theoretical research shows that the dissolution pattern is determined by the injection velocity. At low injection velocities, the effect of diffusion is more dominant than that of convection, and acid reacts with the medium as soon as they contact with each other, giving a face dissolution pattern. At high injection velocities, most of the acid penetrating into the medium before reaction leads to insufficient reaction time so that uniform dissolution pattern is created. At intermediate injection velocities, wormholes are created so that an expected permeability is achieved with minimum acid volume.

Many researchers studied the effect of injection velocities on dissolution patterns through injecting acid into linear cores at constant rate. Daccord (1987), and Daccord et al. (1993a, 1993b) studied the dissolution pattern through injecting water into both radial and linear cores made of plaster, which showed the dissolution pattern changed with the injection velocities. High injection rates created the uniform dissolution pattern, low ones created the face dissolution pattern, and intermediate ones the wormholes. Linear limestone and dolomite core experiments were conducted by Hoefner and Fogler (1988) to study the dissolution pattern at different injection rates, the results are very similar to those obtained by Daccord (1987). Other researchers also studied the effect of different parameters on wormhole formation. Frick et al. (1994) studied the effect of permeability, injection rate and acid concentration through radial core experiments. Buijse (2000) used large diameter cores to investigate the optimal injection velocity and

* Corresponding author.
E-mail addresses: liuming1104@gmail.com (M. Liu), zhangsc@cup.edu.cn (S. Zhang), moujianye@cup.edu.cn (J. Mou).

0920-4105/$ - see front matter © 2012 Elsevier B.V. All rights reserved.
http://dx.doi.org/10.1016/j.petrol.2012.06.021

Nomenclature

a_0	the initial interfacial area of the medium (m^{-1})
a_v	the interfacial area of the medium (m^{-1})
A_v	dimensionless interfacial area
C_0	the initial acid concentration (mol/L)
c_f	dimensionless cup-mixing concentration of the acid in the fluid phase
C_f	cup-mixing concentration of the acid in the fluid phase (mol/L)
c_s	dimensionless concentration of the acid at the fluid–solid phase
C_s	the concentration of the acid at the fluid–solid phase (mol/L)
Da	Damköhler number, defined as the ratio of convection time to reaction time based on the length scale of the core
D_{eR}	effective dispersion coefficient in the fluid phase in the radial direction (m^2/s)
$D_{e\theta}$	effective dispersion coefficient in the fluid phase in the circumferential direction (m^2/s)
D_m	effective molecular diffusivity of the acid species (m^2/s)
D_r	dimensionless effective dispersion coefficient in the fluid phase in the radial direction
D_θ	dimensionless effective dispersion coefficient in the fluid phase in the circumferential direction
h	the formation thickness (m)
i	the number of the ith grid in the radial direction
K	permeability of the medium (μm^2)
K_0	the initial average permeability of the medium (μm^2)
k	dimensionless permeability of the medium
k_c	local mass transfer coefficient (m/s)
k_d	the permeability of the damaged zone (μm^2)
k_r	the reservoir permeability without damage (μm^2)
k_s	reaction rate constant (m/s)
k_{wh}	the permeability of the wormhole zone (μm^2)
l_r	correlation length in the radial direction
l_θ	correlation length in the circumferential direction
m	the ratio of pore length to pore diameter
N_{ac}	acid capacity number, defined as the volume of solid dissolved per unit volume of the acid
NX	the total number of the grids in the radial direction
N_r	number of vugs in the radial direction
N_θ	number of vugs in the circumferential direction
p	dimensionless formation pressure
P	formation pressure (MPa)
Pe	radial Peclet number, defined as the ratio of radial diffusion time to convection time
P_e	the pressure at the outlet (MPa)
P_{wf}	the bottom hole pressure (MPa)
$P_{wf,\ ideal}$	the ideal bottom hole pressure (MPa)
$P_{wf,\ real}$	the real bottom hole pressure (MPa)
q	the injection rate (m^3/s)
r_d	the distance from the front of the damaged zone to the wall (m)
r_e	the external radius (m)
Re_p	pore scale Reynold's number
r_o	the internal radius (m)
r_{p0}	the initial average pore radius of the medium (m)
r_w	the wellbore radius (m)
r_{wh}	the distance from the wormhole front to the wall (m)
$R(C_s)$	the rate of the dissolution reaction, for single step irreversible reaction $R(C_s)=k_sC_s$ (m mol/s/L)
Sc	Schmidt number, defined as the ratio of momentum diffusivity to mass diffusivity
Sh	Sherwood number, defined as the ratio of convective to diffusive mass transport
Sh_∞	asymptotic Sherwood number
S_{after}	the skin factor after wormhole breaks through the damaged zone
S_{before}	the skin factor before wormhole breaks through the damaged zone
t'	time (s)
t	dimensionless time
u	dimensionless velocity in the radial direction
$\|U\|$	magnitude of fluid velocity (m/s)
u_0	the inlet velocity (m/s)
u_r	the velocity in the radial direction (m/s)
u_θ	the velocity in the circumferential direction (m/s)
v	dimensionless velocity in the circumferential direction
ϕ^2	Thiele modulus, defined as the ratio of diffusion time to reaction time based on the initial pore size

Greek symbols

α	dissolving power of the acid defined as grams of solid dissolved per mole of acid reacted (g/mol)
α_{os}	constant depend on pore geometry ($\alpha_{os}=1.0$ for packed-bed of spheres)
α_w	dimensionless wellbore radius
β	exponent determined from experiment
ε	porosity of the medium
ε_0	the initial average porosity of the medium
ζ_p	dimensionless pore radius
η	dimensionless initial pore diameter
λ_r	constant depend on pore geometry ($\lambda_r=0.5$ for packed-bed of spheres)
λ_θ	constant depend on pore geometry ($\lambda_\theta=0.1$ for packed-bed of spheres)
μ	viscosity of the fluid phase (mPa s)
ξ	dimensionless wormhole length in the radial direction
ρ_s	density of the solid phase (kg/m^3)
σ	standard deviation
Φ^2	macroscopic Thiele modulus which is core-scale equivalent of the micro-Thiele modulus

pore volume to breakthrough. Bazin (2001) studied the effect of permeability, temperature and length of the core on optimal conditions. Golfier et al. (2002) also performed experiments similar to Daccord (1987) by injecting under-saturated salt solution into a porous medium made of salt grains and observed similar dissolution patterns.

Three main mathematical models were developed to describe the above experimental results, namely the capillary tube model, the network model and the averaged model. The capillary tube model which was developed by Buijse (2000), Gdanski (1999), Huang et al. (1997, 1999), and Hung et al. (1989) focused on the effect of fluid leakage and the mechanisms of transport and reaction inside the wormhole, but overlooked the condition for wormhole formation because wormholes were assumed to be there already. Fredd and Fogler (1998) and Hoefner and Fogler (1988) developed a network model to represent porous medium

as a network of tubes. The model captured the dissolution pattern through the increase in tube radius, but the results were very different from those of experiments. the averaged model, also known as the continuum model, was based on both Darcy scale and pore scale. Darcy scale was much larger than the pore scale but smaller than the core scale. To describe dissolution at the Darcy scale, we needed information from the pore scale model which could be obtained from semi-empirical equations. The prediction of the pore scale model depends on the pore structures that changed with dissolution. Therefore, the information of the two scale models could be continuously transferred. Golfier et al. (2002) and Liu et al. (1997) have done some contributions to the model. Panga et al. (2005) further developed the model and studied the effect of reaction kinetics and heterogeneity in the linear model. Kalia and Balakotaiah (2007) extended the model to simulate the radial flow. They studied the effects of convection and diffusion on dissolution patterns and heterogeneities on wormholing in radial model. Kalia and Balakotaiah (2009) used the linear model to simulate kinds of heterogeneities of porous medium and studied the effect of them on reactive dissolution. In the model, all values of porosities are generated by adding a random number uniformly distributed in a range to the mean value of initial porosity, hereinafter this method referred to as the uniform distribution method. However, many literatures (Chierici, 1994; Greenkorn, 1983; Hollis et al., 2010; Schoenfelder et al., 2008) show that the porosity distributions in real rocks obey the normal law.

Izgec et al. (2008, 2009) investigated the effect of vugs on wormholing through experiments and mathematical model. They found that the acid injected into vuggy rocks follows a preferential pathway guided by the vug network and the pore volume to breakthrough decreased with the increase of the proportion of vugs in the domain. However, the mathematical model did not involve the acid–rock reaction.

In this paper, we use a new method to generate normally distributed porosities instead of uniform distributions in the two-scale radial continuum model extended by Kalia and Balakotaiah (2007), we refer to this method as the normal distribution method. First, the normal distribution method for porosities is introduced and compared with the uniform distribution method. Second, the heterogeneity parameters introduced by the new method and the effect of them on dissolution patterns are investigated. Third, the effect of completion and vugs is studied and the pressure response for different completions and dissolution patterns is analyzed. Finally, an apparent skin factor model is developed to study the skin factor change with wormhole propagation.

2. Mathematical model

A two-scale continuum model is used in this study to simulate the 2D radial flow. The model was first developed by Panga et al. (2005) and extended to radial flow by Kalia and Balakotaiah (2007). We present the model in this section. Except for Eq. (24) which is used to generate normally distributed porosities, others (Eqs. (1)–(23) and Eq.(25)) are borrowed from Kalia and Balakotaiah (2007).

2.1. Darcy scale model

Darcy scale model describes the convection, diffusion and reaction mechanisms as it follows:

$$(u_r,v_\theta)=-\frac{K}{\mu}\left(\frac{\partial P}{\partial r},\frac{1}{r}\frac{\partial P}{\partial \theta}\right) \tag{1}$$

$$\frac{\partial \varepsilon}{\partial t'}+\frac{1}{r}\frac{\partial}{\partial r}(ru_r)+\frac{1}{r}\frac{\partial u_\theta}{\partial \theta}=0 \tag{2}$$

$$\frac{\partial(\varepsilon C_f)}{\partial t'}+\frac{1}{r}\frac{\partial}{\partial r}(ru_rC_f)+\frac{1}{r}\frac{\partial}{\partial \theta}(u_\theta C_f) =\frac{1}{r}\frac{\partial}{\partial r}\left(r\varepsilon D_{eR}\frac{\partial C_f}{\partial r}\right)+\frac{1}{r}\frac{\partial}{\partial \theta}\left(\frac{\varepsilon D_{e\theta}}{r}\frac{\partial C_f}{\partial \theta}\right)-k_c a_v(C_f-C_s) \tag{3}$$

$$k_c(C_f-C_s)=R(C_s) \tag{4}$$

$$\frac{\partial \varepsilon}{\partial t'}=\frac{R(C_s)a_v\alpha}{\rho_s} \tag{5}$$

2.2. Pore scale model

In order to solve the Darcy scale model, pore information due to reaction is required. A property–structure approach is adopted by Kalia and Balakotaiah (2007) and described as follows:

$$\frac{K}{K_0}=\frac{\varepsilon}{\varepsilon_0}\left(\frac{\varepsilon}{\varepsilon_0}\left(\frac{1-\varepsilon_0}{1-\varepsilon}\right)\right)^{2\beta} \tag{6}$$

$$\frac{r_p}{r_{p0}}=\sqrt{\frac{K\varepsilon_0}{\varepsilon K_0}} \tag{7}$$

$$\frac{a_v}{a_0}=\frac{\varepsilon r_{p0}}{\varepsilon_0 r_p} \tag{8}$$

Mass transfer coefficient is influenced by pore structure and reaction rate. The effect of these parameters on mass transfer coefficient was studied in detail (Balakotaiah and West, 2002; Gupta and Balakotaiah, 2001):

$$Sh=\frac{2k_c r_p}{D_m}=Sh_\infty+\frac{0.7}{m^{1/2}}Re_p{}^{1/2}Sc^{1/3} \tag{9}$$

To describe the dispersion in the acid phase, following equations can be used:

$$D_{eR}=\alpha_{os}D_m+\frac{2\lambda_r|U|r_p}{\varepsilon} \tag{10}$$

$$D_{e\theta}=\alpha_{os}D_m+\frac{2\lambda_\theta|U|r_p}{\varepsilon} \tag{11}$$

2.3. Non-dimensional process

Dimensionless variables used to non-dimensionalize Eqs. (1)–(11) are expressed as follows:

$$\begin{aligned}
&\xi=\frac{r}{r_e},\quad \alpha_w=\frac{r_o}{r_e},\quad u=\frac{u_r}{u_0},\quad v=\frac{u_\theta}{u_0},\quad t=\frac{t'}{r_e/u_0},\\
&\zeta_p=\frac{r_p}{r_{po}},\quad A_v=\frac{a_v}{a_0}k=\frac{K}{K_0},\quad c_f=\frac{C_f}{C_0},\quad c_s=\frac{C_s}{C_0},\\
&p=\frac{P-P_e}{\mu u_0 r_e/K_0},\quad \eta=\frac{2r_{po}}{r_e},\quad \phi^2=\frac{2k_s r_{po}}{D_m}\\
&Da=\frac{k_s a_0 r_e}{u_0},\quad N_{ac}=\frac{\alpha C_0}{\rho_s},\quad Pe=\frac{u_0 r_e}{D_m},\quad \Phi^2=DaPe=\frac{k_s a_0 {r_e}^2}{D_m}
\end{aligned} \tag{12}$$

The non-dimensional forms of the Eqs. (1)–(11) are shown as:

$$(u,v)=-\left(k\frac{\partial p}{\partial \xi},\frac{k}{\sigma}\frac{\partial p}{\partial \theta}\right) \tag{13}$$

$$\frac{\partial \varepsilon}{\partial t}-\frac{1}{\xi}\frac{\partial}{\partial \xi}\left(\xi k\frac{\partial p}{\partial \xi}\right)-\frac{1}{\xi}\frac{\partial}{\partial \theta}\left(\frac{k}{\xi}\frac{\partial p}{\partial \theta}\right)=0 \tag{14}$$

$$\frac{\partial(\varepsilon c_f)}{\partial t}+\frac{1}{\xi}\frac{\partial}{\partial \xi}(\xi uc_f)+\frac{1}{\xi}\frac{\partial}{\partial \theta}(vc_f) =\frac{1}{\xi}\frac{\partial}{\partial \xi}\left(\xi D_r\frac{\partial c_f}{\partial \xi}\right)+\frac{1}{\xi}\frac{\partial}{\partial \theta}\left(\frac{D_\theta}{\xi}\frac{\partial c_f}{\partial \theta}\right)-\frac{DaA_v c_f}{1+(\phi^2\zeta_p/Sh)} \tag{15}$$

$$\frac{\partial \varepsilon}{\partial t} = \frac{DaN_{ac}A_v c_f}{1+(\phi^2\zeta_p/Sh)} \tag{16}$$

$$k = \frac{\varepsilon}{\varepsilon_0}\left(\frac{\varepsilon}{\varepsilon_0}\left(\frac{1-\varepsilon_0}{1-\varepsilon}\right)\right)^{2\beta} \tag{17}$$

$$\zeta_p = \sqrt{k\frac{\varepsilon_0}{\varepsilon}} \tag{18}$$

$$A_v = \frac{\varepsilon}{\zeta_p \varepsilon_0} \tag{19}$$

$$D_r = \frac{\alpha_{os}\varepsilon Da}{\Phi^2} + \lambda_r |U|\zeta_p \eta \quad D_\theta = \frac{\alpha_{os}\varepsilon Da}{\Phi^2} + \lambda_\theta |U|\zeta_p \eta \tag{20}$$

The boundary and initial conditions are as follows:

$$-k\frac{\partial p}{\partial \xi} = 1, \quad c_f = 1 \ \text{ at } \ \xi = \alpha_w \tag{21}$$

$$p = 0, \quad \frac{\partial c_f}{\partial \xi} = 0 \ \text{ at } \ \xi = 1 \tag{22}$$

$$c_f = 0 \ \text{ at } \ t = 0 \tag{23}$$

$$\varepsilon = \begin{cases} 0.99, \varepsilon \geq 0.99 \\ \varepsilon_0 + \varepsilon_0 \sigma \hat{G}(l_r, l_\theta), 0.005 < \varepsilon < 0.99 \ \text{ at } \ t = 0 \\ 0.005, \varepsilon \leq 0.005 \end{cases} \tag{24}$$

$$p(\xi,\theta) = p(\xi,\theta+2\pi), \quad c_f(\xi,\theta) = c_f(\xi,\theta+2\pi) \ \text{ at } \ \theta = 0 \tag{25}$$

Compared with the uniform distribution method in porosity field to simulate the heterogeneity, the porosity distribution in the porous medium is assumed to follow the normal law in this paper. The correlation length is a measure of the range over which fluctuations in one region of space are correlated with those in another region. Two points which are separated by a distance larger than the correlation length will each have fluctuations which are relatively independent, that is, uncorrelated. $\hat{G}(l_r,l_\theta)$ is the Gaussian distribution whose correlation lengths are l_r and l_θ in the radial and circumferential directions respectively. We can assign different values of l_r and l_θ to simulate different correlation lengths. For example, $l_r=5$ and $l_\theta=3$ (hereinafter referred to as $l_r/l_\theta=5/3$) mean five continuous grids and three continuous grids are correlated in the radial and circumferential direction, respectively. σ is the standard deviation of the porosity distribution. As shown in Fig. 1, the greater the standard deviation, the values more evenly distributed. Almost all of the generated values fall in a narrow range as the standard deviation is very small, which means very weak heterogeneity. Heterogeneity is increased as the standard deviation is increased. According to the characteristics of normal distribution, we set threshold value for porosity to validate simulation, shown as Eq. (24). The porosity data are generated by GSLIB (Deutsch and Journel, 1998).

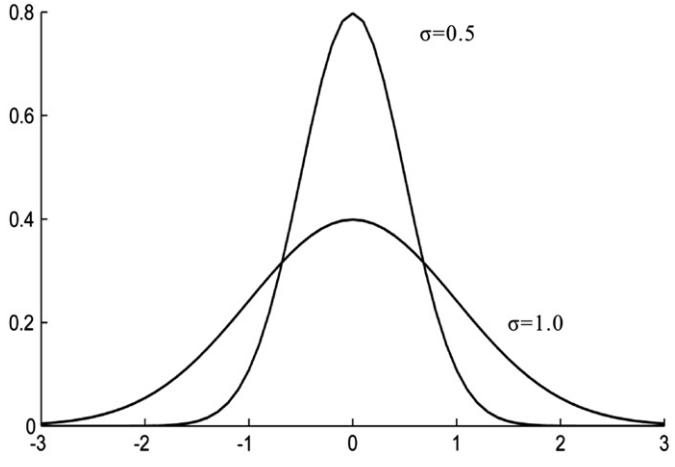

Fig. 1. Normal curves for different standard deviations.

A constant flow rate boundary condition is imposed at the inlet and there are 120 and 200 grids in radial and circumferential directions respectively. All the values needed for the model simulation shown in Table 1 are fixed unless otherwise stated.

3. Comparison of two different porosity distribution methods

The influence of different porosity distribution methods on wormhole propagation may be different. Although the real porosities of a core are distributed in a normal way, the uniform distribution method is used commonly in the literature. Therefore, the comparison between the two methods is important to understand which method is better to study the wormholing mechanism and whether the results got from the former literatures are reasonable.

The data of core size and injection condition are based on the two experiments conducted by Tardy et al. (2007). Other parameters in the model use the corresponding values in Table 1. Fig. 2 shows dissolution patterns in porosity, in which the porosities of case #1 are generated by the normal distribution method and those of case #2 are generated by the uniform distribution method. The indication of breakthrough in this paper is pressure at the inlet drops to one hundredth of the initial value. From the figure, we can see that only one dominant wormhole breaks through the cores and other wormholes are not well developed as the porosities are normally distributed. However, when porosities are uniformly distributed wormholes are more evenly competed and face dissolution is formed at the inlet. Not-well-developed wormholes are relatively well developed compared to case #1. The differences between the two methods are caused by the magnitude of heterogeneity. Normally distributed porosities contain much larger and smaller values, which is different from the uniformly distributed porosities whose values are rigorously restricted in a certain range, Fig. 2. Therefore, the heterogeneity of normally distributed porosities is stronger than that of uniformly distributed porosities. Strong heterogeneity makes acid randomly flow into the big porosity region and wormholes unevenly develop. Once a dominant wormhole forms, other not-well-developed wormholes hardly propagate due to most acid flowing into the dominant wormhole. Wormhole patterns obtained from Tardy's experiments are shown in Fig. 3. Comparing Fig. 2 with Fig. 3, we can see that the wormhole structures obtained from normally distributed porosities are more similar to the ones obtained from the Tardy's experiments.

Table 1
Model parameters and corresponding values.

K_0 (μm^2)	ε_0 (dimensionless)	μ (mPa s)	r_e (m)	r_o (m)	β (dimensionless)	k_s (m/s)	D_m (m^2/s)	r_{po} (10^{-6} m)	a_0 (cm^{-1})	α (g/mol)	C_0 (mol/L)	ρ_s (kg/m^3)	ρ_l (kg/m^3)
0.01	0.15	10	0.4	0.1	1	2×10^{-3}	3×10^{-9}	1	50	50	4.4	2200	1000

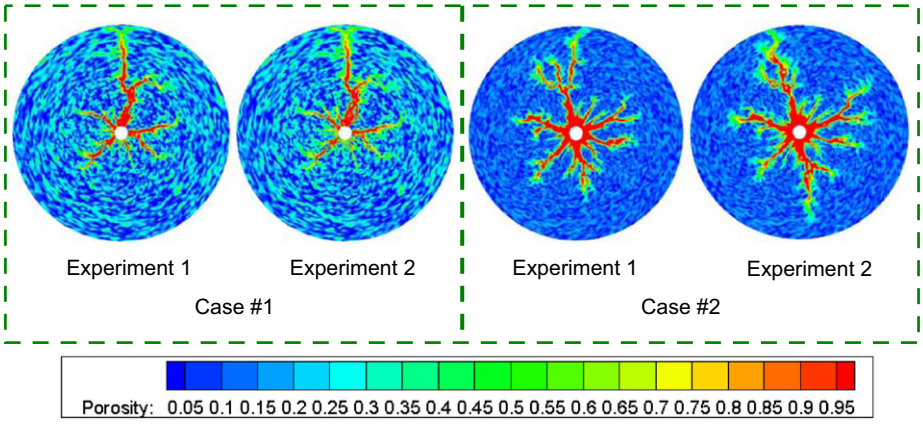

Fig. 2. Dissolution patterns in porosity for two cases at $l_r/l_\theta=1/1$ and $\sigma=1.0$, the porosities of cases #1 and #2 are generated by the normal distribution method and the uniform distribution method respectively.

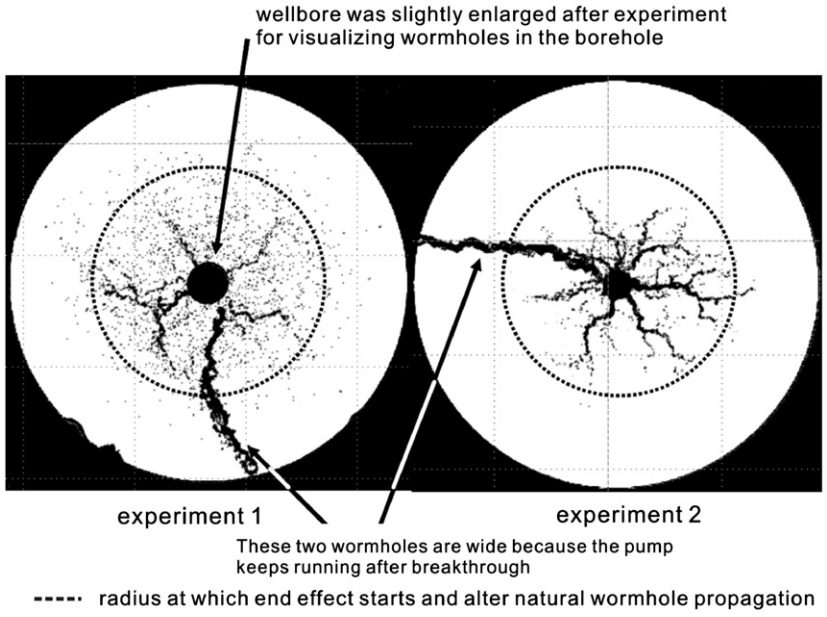

Fig. 3. Wormhole patterns observed in Tardy's experiments: the external radius, internal radius and height of the cores in the two experiments are 2.77 in., 0.125 in. and 2.3 in. respectively. Compared to the core diameter, little height means radial flow in the cores.

Fig. 4 shows breakthrough curves for the two different porosity generation methods. Pore volume to breakthrough, PV_{bt}, is defined as the ratio of acid injection volume to total pore volume. Results of core experiments show that the optimal pore volume to breakthrough for 15 wt% (4.4 mol/L) HCl is about 1 or less for most cases (Bazin, 2001; Fredd et al., 1997; Fredd and Fogler, 1998; Furui et al., 2010; Ziauddin and Bize, 2007), which indicates very fast propagation velocity of wormhole. From Fig. 4, the optimal pore volume to breakthrough for normally distributed porosities is about 1 which is much closer to the real cases shown in the above literatures. According to comparing the wormhole structures and pore volume to breakthrough with the published experimental results, we can see that the normal distribution method is more capable of producing the real conditions than the uniform distribution method.

A difference is that the optimal Damköhler number for the normal distribution method is larger than that for the uniform distribution method. As the Damköhler number is inversely proportional to the injection velocity, the required injection velocity for the

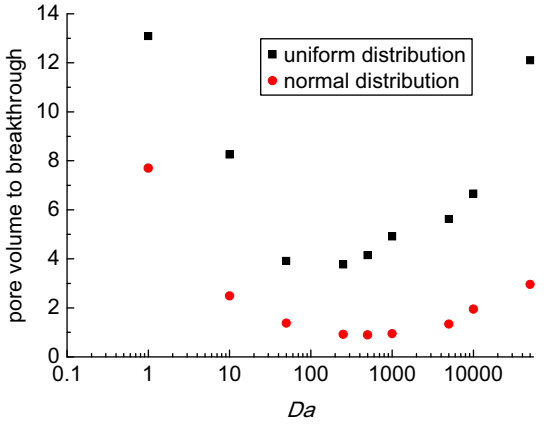

Fig. 4. Breakthrough curves for two different porosity generation methods.

normal distribution method is less than that for the uniform distribution method. All of these are caused by strong heterogeneity for porosities generated by the normal distribution method.

Experienced experts are able to find that the normal distribution method is essential if they want to successfully simulate the characteristics of self-diverting acid in carbonate acidizing. Self-diverting acid can be self-viscosified with its consumption. Once it consumes to some extent and the pH increase to a certain value, self-diverting acid viscosifies itself quickly. Huge resistance caused by great viscosity diverts acid to other low permeability formations so that all formations are able to be treated. Experiments show that the viscosity of spent self-diverting acid depends on pH, concentrations of cation and surfactant. Pressure at the inlet builds up in a long injection time and builds down in the last short injection time. Since cation and surfactant flow with the spent acid and the pressure builds up between the wormhole front and spent acid front, the simulation of wormhole propagation velocity is very important. If wormhole propagation velocity is too slow, the spent acid front arrives at the outlet before wormhole develops a little. Then pressure builds up in a short injection time and builds down in the last long injection time before breakthrough, it is not able to simulate the real pressure change. Since the simulated wormhole propagation velocity with the normal distribution method is faster than the uniform distribution method, it is necessary to choose the new method to make our simulation be closer to the real condition.

4. Effect of heterogeneity

4.1. Effect of correlation length

Correlation length in the radial or circumferential direction represents different heterogeneity of a reservoir. The magnitude represents the number of grids correlated. In a 2D radial model, bigger correlation length in radial direction implies stronger continuity in the radial direction, and vice versa. In real formations, the correlation lengths in two directions are usually different from each other. The wormhole propagation will be changed with a different correlation system which plays an important role in acidizing design. Fig. 5 shows the dissolution patterns in porosity at $l_r/l_\theta=1/3$ and $l_r/l_\theta=1/10$, and Fig. 6 shows the dissolution patterns at $l_r/l_\theta=3/1$ and $l_r/l_\theta=10/1$. From Fig. 5, wormholes almost propagate along the radial direction without any effect of correlation in the circumferential direction at $l_r/l_\theta=1/3$. However, wormholes propagate away from the radial direction which leads to thicker

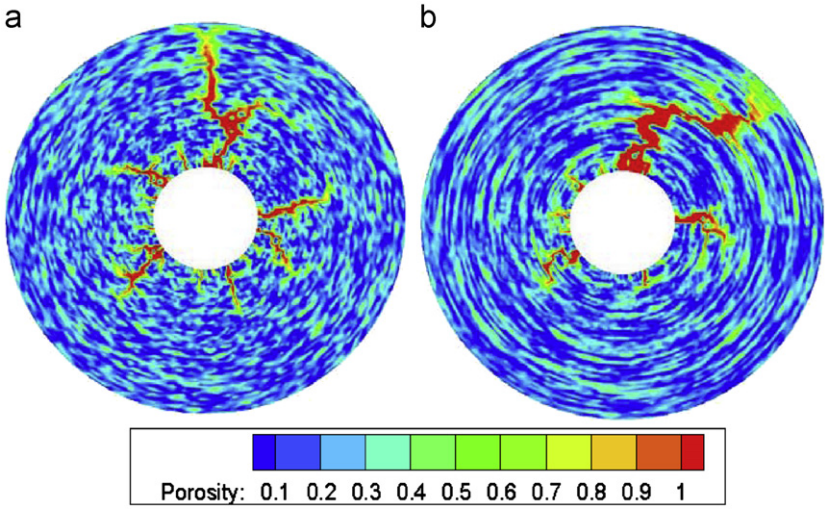

Fig. 5. Dissolution patterns in porosity for two different radial correlations (a) $l_r/l_\theta=1/3$ and (b) $l_r/l_\theta=1/10$.

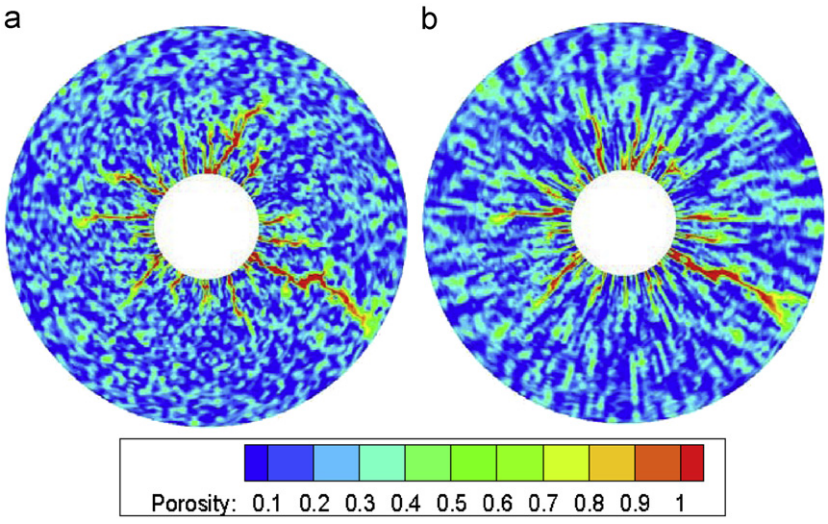

Fig. 6. Dissolution patterns in porosity for two different circumferential correlations (a) $l_r/l_\theta=3/1$ and (b) $l_r/l_\theta=10/1$.

wormhole at $l_r/l_\theta=1/10$, which means wormholes are considerably influenced by the strong correlation in the circumferential direction. The radial correlated porosities increase the number of wormholes formed and make wormholes be thinner. Since big porosities at the inlet are correlated in the radial direction, acid flowing into these channels simultaneously creates many not-well-developed wormholes and only one dominant wormhole breaks through. Compared to the case of $l_r/l_\theta=3/1$, wormholes in case of $l_r/l_\theta=10/1$ are thinner and shorter.

4.2. Effect of initial porosity

From Eq. (24), the porosity distribution depends on initial porosity ε_0. Based on the normal law, high initial porosity leads to the results of increasing number of super high and super low porosities. Then the heterogeneity is stronger. Due to different pore volumes for different initial porosities, we use total acid injection volume instead of pore volume to breakthrough. Fig. 7 is the breakthrough curves for different initial porosities at $l_r/l_\theta=1/1$ and $\sigma=1.0$. From the figure, the total acid injection volume and optimal injection velocity decrease with the increase of initial porosity. This is because the bigger the porosity, the stronger the heterogeneity. Strong heterogeneity leads to an uneven competition among acid and wormhole is formed along the big porosity channel.

4.3. Effect of standard deviation

It is indicated from Fig. 1 that small standard deviation leads to weak heterogeneity and big standard deviation leads to strong heterogeneity. From Fig. 8, it can be seen that the heterogeneity is weak when the standard deviation is small so that the wormholes compete evenly to break through the domain. Therefore, the number of wormholes is high and the wormholes are straight and thick. The number of wormholes becomes less and the wormholes are tortuous with the increase of standard deviation. The tortuosity of wormholes is caused by strong heterogeneity. Fig. 8(d) is the same as Fig. 5(a).

Fig. 9 is the optimal breakthrough curves for two different initial porosities at $l_r/l_\theta=1/1$. The optimal pore volume to breakthrough, $PV_{bt,opt}$, is the least pore volume to breakthrough which correspondences to the optimal injection velocity or optimal Damköhler number. From the figure, we can see that a critical value of standard deviation exists for a certain initial porosity, below which the optimal pore volume to breakthrough is not sensitive to the standard deviation, above which the optimal pore volume to breakthrough decreases sharply. The optimal pore volume to breakthrough is least when the standard deviation is 1.

5. Effect of completion

5.1. Perforation length

Perforation completion is a common completion in reservoir development. Perforation connects the wellbore with the reservoir in order for hydrocarbons to flow into the wellbore. Since other parts of wellbore cannot connect the reservoir, the perforation dimension plays an important role in production. To study the effect of the perforation length on dissolution pattern, we

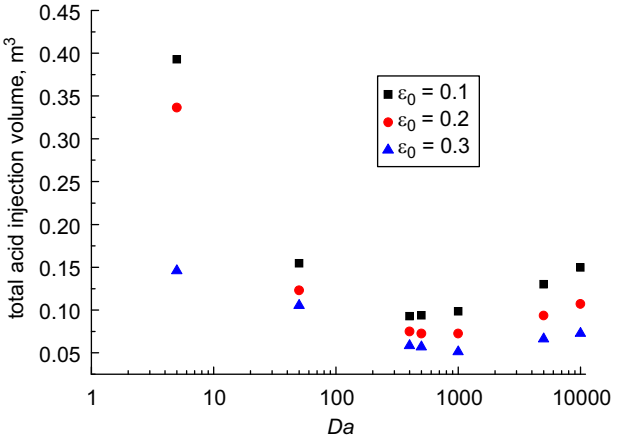

Fig. 7. Breakthrough curves for different initial porosities.

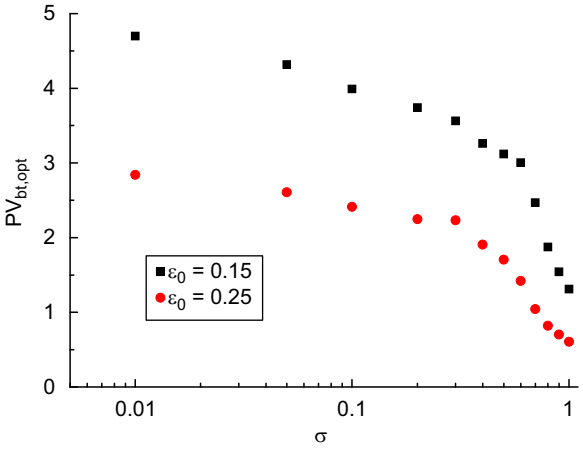

Fig. 9. Optimal pore volume to breakthrough change with the standard deviation for different initial porosities at $l_r/l_\theta=1/1$.

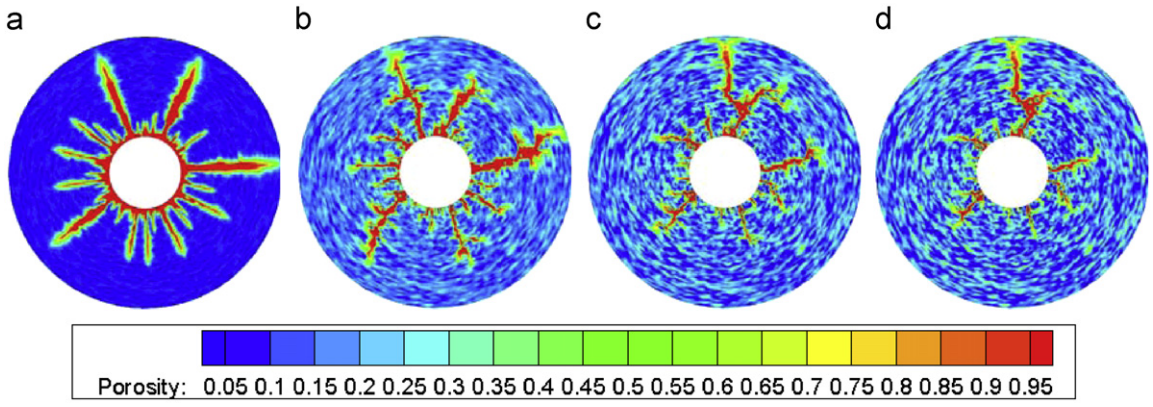

Fig. 8. Dissolution patterns for different standard deviations at $l_r/l_\theta=1/1$ (a) $\sigma=0.1$; (b) $\sigma=0.5$; (c) $\sigma=0.8$; and (d) $\sigma=1.0$.

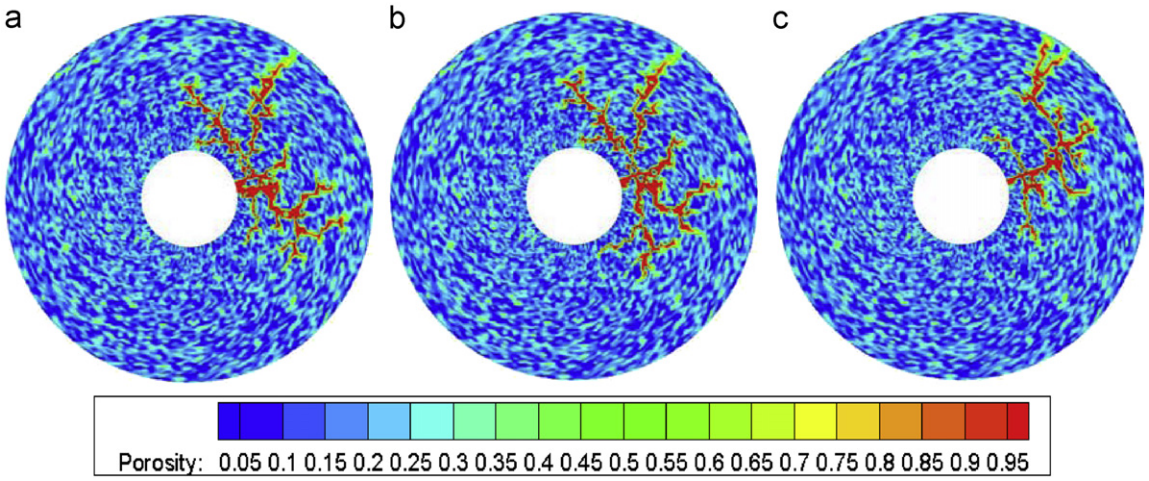

Fig. 10. Dissolution patterns for different perforation lengths of (a) L_{per}=25 mm; (b) L_{per}=50 mm; and (c) L_{per}=100 mm.

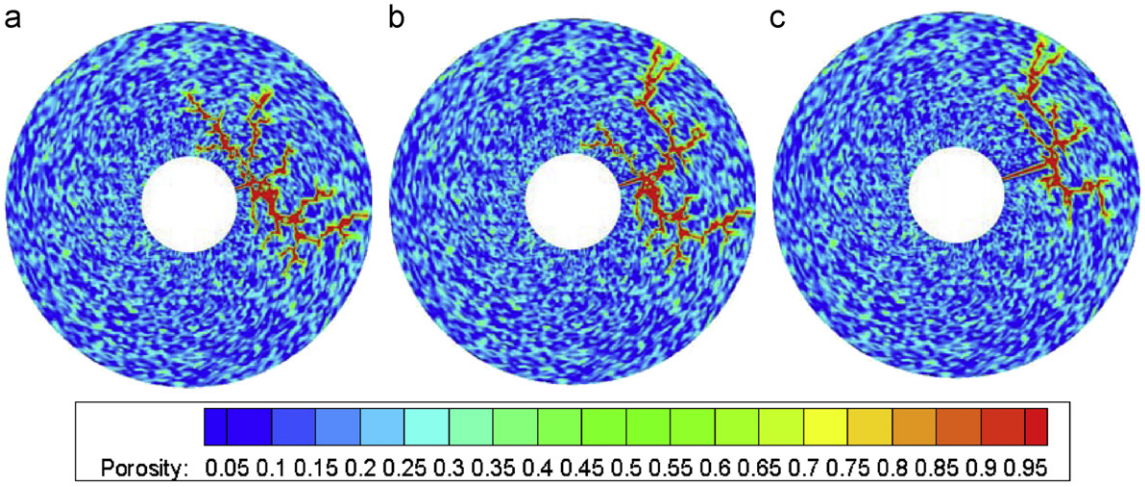

Fig. 11. Dissolution patterns for damaged perforation whose lengths are (a) $_{Lper'}$=25 mm; (b) $L_{per'}$=50 mm; and (c) $L_{per'}$=100 mm.

simulate different perforation lengths. Perforation is represented by grids whose initial porosities are 0.95. Fig. 10 shows dissolution patterns in porosity for three different perforation lengths at l_r/l_θ=1/1 and σ=1.0, where L_{per} represents the perforation length. Leakoff occurs in all three cases. Wormholes are seriously branched because of serious leakoff in the circumferential direction. From the figure, acid leakoff decreases and breakthrough time delays with the decrease of perforation length. Regardless of heavy leakoff for long perforation, the advantage of perforation which creates a high permeability channel plays a dominate role in wormholing.

5.2. Perforation damage

Damage cannot be avoided during perforating. We cannot simulate partial damage because of inadequate information about leakoff and damage level. We assume that perforation is damaged so that acid is not able to leak off from the two sides of it and can only flow through it. The permeabilities of the grids next to the perforation in the circumferential direction are set to zero. Fig. 11 shows the dissolution patterns in porosity for three different damaged perforations at l_r/l_θ=1/1 and σ=1.0, where $L_{per'}$ represents the length of damaged perforation. The wormholes patterns are similar to those of undamaged perforations with short length, such as $L_{per'}$=25 mm. Fig. 12 shows the breakthrough curves for

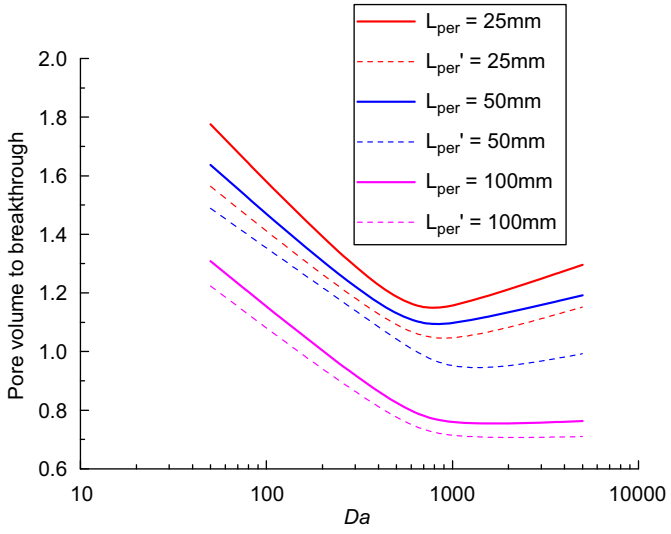

Fig. 12. Breakthrough curves for different perforation conditions.

different perforation conditions. The pore volume to breakthrough decreases with the increase of perforation length both for undamaged and damaged perforation. For a certain perforation length, the pore volume to breakthrough of undamaged

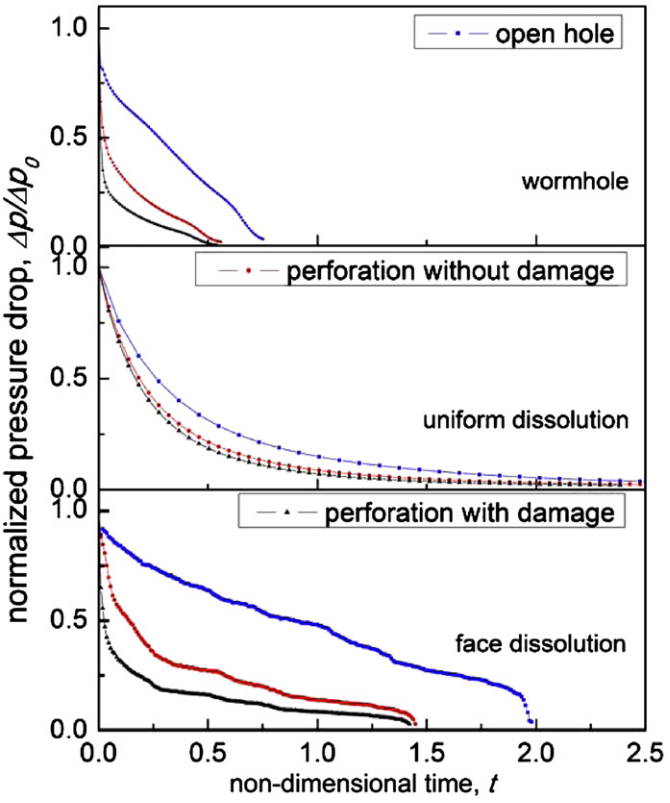

Fig. 13. Normalized pressure drop for different completions and dissolution patterns, and the perforation length is 25 mm for perforation completion case.

perforation is bigger than that of damaged perforation. The reason is that leakoff of acid for undamaged perforation wastes a part of injected acid. However, there is no reason to believe that damage is necessary to minimize acid injection volume. We shall avoid damage during perforating because the damage may occur in the head of perforation to block it. Moreover, the difference of pore volume to breakthrough between undamaged and damaged perforation is little.

5.3. Pressure response

During acid dissolving rock, the pressure at the inlet declines from the initial value to the value defined from the breakthrough criterion. The pressure drop curves are different from each other according to different dissolution patterns and completions. To study this effect, we simulate the effect of different completions on pressure drop, as shown in Fig. 13. From the curves, the pressure for open-hole completion declines faster than that for perforation completion. Perforation with damage reduces the acid leakoff so that wormhole propagates faster and the pressure declines more quickly. When face dissolution pattern is formed, a sharp decline in pressure drop occurs at the end. This is because the spent acid front is ahead of the reaction front and the distance between them is short. When uniform dissolution pattern is formed, the pressure declines slowly due to the wide reaction front.

6. Effect of vugs

Vugs are developed in vuggy reservoirs. Compared to cases without vugs, wormholes propagation can be influenced when acid flows through vugs. Vugs which commonly have big porosity affect the pressure distribution in the domain. A small vug rarely affects wormhole propagation, only extra-large vug or a sequential of continuous vugs can affect acid flow path. Vugs are represented by grids whose initial porosities are 0.95. Fig. 14 shows wormhole propagation for different vug distributions. N_r and N_θ represent the number of vugs in the radial and circumferential direction respectively. At $N_r=3$ and $N_\theta=15$, the dissolution pattern is nearly not affected by vugs. At $N_r=11$ and $N_\theta=15$, wormholes change a lot with the increase of vugs in radial direction. Since vugs in the radial direction are very close to each other, acid tends to flow along the vugs array. At $N_r=6$ and $N_\theta=40$, the number of wormholes increase with the increase of the number of vugs in the circumferential direction. Many not-well-developed wormholes are formed because of the large number of vugs at the inlet. So, vugs can influence the wormhole propagation when they are so close to each other that acid is able to get into the next vug before diverting due to heterogeneity.

7. Skin factor model

To investigate the improvement of acidizing to well production, we assume a damaged well stimulated with acid. Negative skin factor means good flow condition near the wellbore. The permeabilities of zones with wormholes are assumed to be infinite, so wormholes propagating in the damaged zone can decrease the skin factor.

We derive an apparent skin factor model to study the effect of wormhole on skin factor. The top view of wormhole propagation in a damaged well is shown in Fig. 15.

There are two cases according to different wormhole range: (1) wormholes propagate between the wall of the well and the front of the damaged zone; (2) wormholes break through the damaged zone.

(1) $r_{wh} < r_d$

The pressure difference between the outlet and well in the radial flow under the ideal condition (without damage) is expressed as

$$P_e - P_{wf,ideal} = \frac{q\mu}{2\pi k_r h}\ln\frac{r_e}{r_w} \tag{26}$$

Under the real condition, namely there exists damaged zone, the equation is changed as

$$P_e - P_{wf,real} = \frac{q\mu}{2\pi k_{wh} h}\ln\frac{r_{wh}}{r_w} + \frac{q\mu}{2\pi k_d h}\ln\frac{r_d}{r_{wh}} + \frac{q\mu}{2\pi k_r h}\ln\frac{r_e}{r_d} \tag{27}$$

then, the difference between $P_{wf,ideal}$ and $P_{wf,real}$ is the pressure drop due to the skin factor effect. So,

$$\begin{aligned} P_{wf,ideal} - P_{wf,real} &= \frac{q\mu}{2\pi k_r h} S_{before} \\ &= \frac{q\mu}{2\pi k_{wh} h}\ln\frac{r_{wh}}{r_w} + \frac{q\mu}{2\pi k_d h}\ln\frac{r_d}{r_{wh}} + \frac{q\mu}{2\pi k_r h}\ln\frac{r_e}{r_d} - \frac{q\mu}{2\pi k_r h}\ln\frac{r_e}{r_w} \end{aligned} \tag{28}$$

k_{wh} is usually several orders bigger than k_d and k_r and can be taken as infinity, so we finally obtain

$$S_{before} = \frac{k_r}{k_d}\ln\frac{r_d}{r_{wh}} + \ln\frac{r_w}{r_d} \tag{29}$$

(2) $r_d < r_{wh} < r_e$

We can get the skin factor after breakthrough of the damaged zone using the same method:

$$S_{after} = \ln\frac{r_w}{r_{wh}} \tag{30}$$

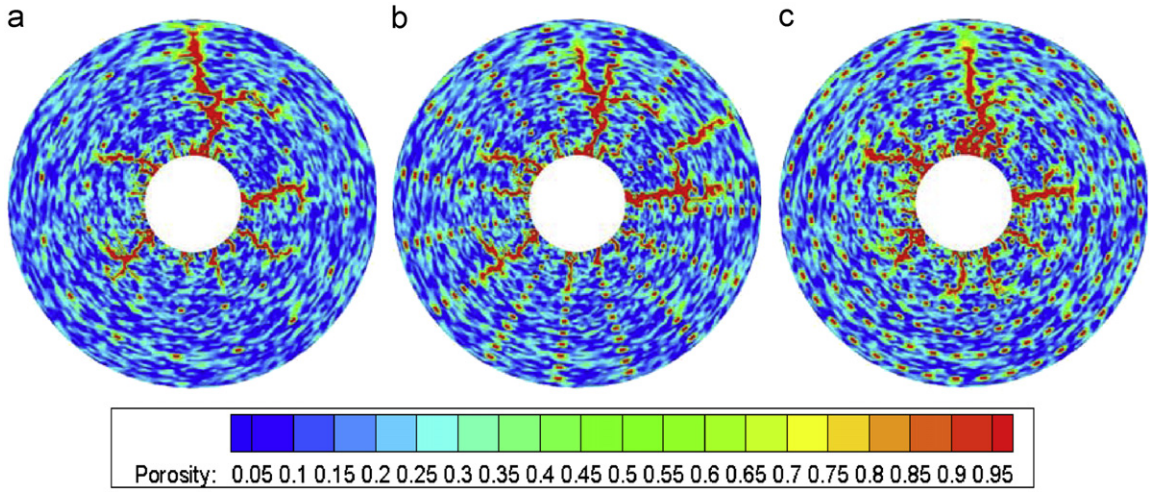

Fig. 14. Dissolution patterns in porosity with different vug distributions (a) $N_r=3$, $N_\theta=15$; (b) $N_r=11$, $N_\theta=15$; and (c) $N_r=6$, $N_\theta=40$.

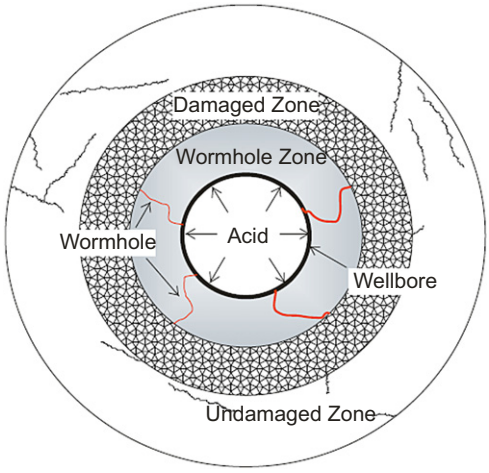

Fig. 15. Top view of wormhole propagation in a damaged well near wellbore.

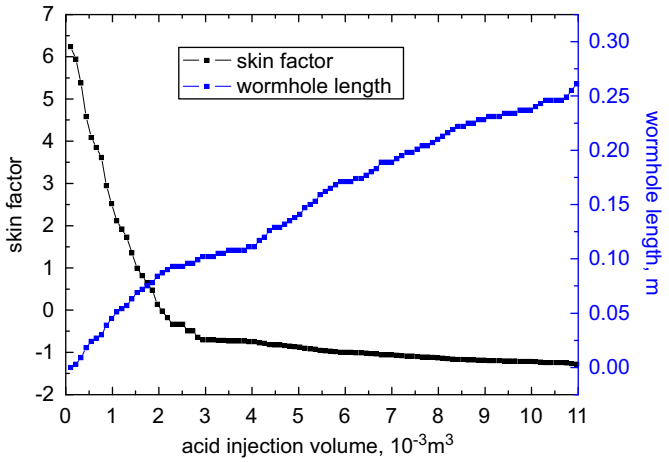

Fig. 16. Skin factor and wormhole length change with the acid injection

From Eqs. (29) and (30), we know that r_{wh} is the only parameter we need to calculate from the two-scale continuum model to define skin factor. Here, we define where the porosity and acid concentration are bigger than 70% and 0.1 mol/L simultaneously respectively as wormholes. The r_{wh} is defined as

$$r_{wh}=\frac{i(r_e-r_w)}{NX} \tag{31}$$

A typical curve between skin factor, wormhole length and acid injection volume is shown in Fig. 16. In this case, $k_r/k_d=10$ and $r_d=0.1$ m. From the curve, we can see that skin factor declines quickly from 6.3 to -0.02 in the first $2\times10^{-3}\,m^3$ of acid injection, then declines slowly to -1.3 in the later acid injection. From Eq. (29), S_{before} equals $\ln(r_w/r_d)$ when r_{wh} is the same as r_d, which means the skin factor comes to a certain value as the wormhole front arrives at the boundary of the damaged zone. After that, the skin factor declines slowly with the wormhole propagation. Note that the total wormhole length which is 0.273 m in this case depends on the calibration conditions of wormhole.

It is also found that the wormhole length increases with time as $r_{wh}=at^b$, a and b are two parameters obtained by the power regression. In this case, $r_{wh}=0.045t^{0.73}$. Daccord and Lenormand (1987) discovered this relationship from experiments and Kalia and Balakotaiah (2007) obtained an approximate value of 0.66 with the uniform distribution method. It is indicated that the wormhole propagation velocity in cores with normally distributed porosities is faster than that with uniformly distributed porosities.

8. Conclusions

The main aim of this work is to investigate the effect of heterogeneity on wormholing with a normal distribution method for porosity. Porosities generated by the new method are close to the real porosity distribution in cores. Due to the characteristics of the normal law, a part of porosities which are too high or low are needed to be truncated. Comparing the breakthrough curves with different porosity generation methods, the pore volume to breakthrough for normally distributed porosities is smaller than that for uniformly distributed porosities, which means less acid injection and faster wormhole propagation velocity. Experimental research suggests that the pore volume to breakthrough is much less than that obtained from Panga's or Kalia's model, which means the normal distribution method is more reasonable to generate porosities. Normally distributed porosities which have too high and low ones represent strong heterogeneity

and uniform distribution method which evenly restricts generated porosities in a certain range inadvertently reduce the heterogeneity.

The effects of three ways of heterogeneities are studied. First, the magnitude of correlation lengths plays an important role in wormholing. Small correlation length in circumferential direction does not affect wormholing very much, but big one thickens the wormhole due to many correlated grids in that direction. Both big and small correlation lengths in radial direction have a huge effect on wormholing. The number of wormholes becomes more and wormholes become thinner. Second, the total acid injection volume for certain injection velocity and optimal injection velocity decrease with the increase of initial porosity. Big initial porosity leads to a result of increase of the number of big porosities for certain standard deviation so that wormholes are created with low injection velocity. Third, the magnitude of standard deviation determines the range of porosity distribution, which means the bigger the standard deviation, the stronger the heterogeneity. A critical value for standard deviation exists for certain initial porosity and correlation length, below which the optimal pore volume to breakthrough is insensitive to the standard deviation, above which the optimal pore volume to breakthrough decreases sharply to a very little value.

Wells with perforation completions should be noticed for varied perforation conditions. Acid can leak off from the two sides of perforation in the circumferential direction. With the increase of perforation length, the wormhole is less branched and the acid volume to breakthrough decreases. We assume the permeabilities of grids next to perforation in the circumferential direction are zero to simulate perforation damage. Compared with the perforation without damage, the pore volume to breakthrough is less for perforation with damage. Since no leakoff occurs along the perforation, all acid injected is used to create wormholes. The faster propagation velocity for the spent acid front than that for the reaction front and the short distance between them are the reasons why the pressure at the end declines sharply for face dissolution pattern. Since the permeability of perforation is high, the pressure for perforation completion declines faster than that for open-hole completion. Vugs are developed in vuggy carbonate reservoirs. Only large number of continuous vugs is able to affect wormholing, small number of non-continuous vugs rarely has an influence on wormholing.

An apparent skin factor model is developed to show the relationship between wormhole propagation and skin factor. Before wormhole breaks through the damage zone, skin factor decreases sharply with the increase of wormhole length. After wormhole breaks through the damage zone, skin factor decreases slowly with the increase of wormhole length. The wormhole length and time follow a power–law relationship as $r_{wh}=at^b$ and the values of a and b are 0.045 and 0.73 respectively.

9. Discussion

It is difficult to simulate the real wormhole propagation velocity in cores even if using the normal distribution method is close to it to a great extent. Structure of wormhole is influenced by grid dimension so that it is impossible to simulate real propagation velocity of wormhole due to a limited number of grids in numerical simulation. The mechanisms of sharp pressure drop at breakthrough and the self-viscosifying process for self-diverting acid are not fully understood. Therefore, how to characterize the self-diverting acid during acidizing is the next work that will be pursued in the future.

Acknowledgment

This work was supported by National Science and Technology Major Project of China. We thank LI Shuang-Ming of Sinopec for his participation with the project.

References

Balakotaiah, V., West, D.H., 2002. Shape normalization and analysis of the mass transfer controlled regime in catalytic monoliths. Chem. Eng. Sci. 57 (8), 1269–1286.
Bazin, B., 2001. From matrix acidizing to acid fracturing: a laboratory evaluation of acid/rock interactions. SPE Prod. Facilities 16 (1), 22–29.
Buijse, M.A., 2000. Understanding wormholing mechanisms can improve acid treatments in carbonate formations. SPE Prod. Facilities 15 (3), 168–175.
Chierici, G.L., 1994. Principles of Petroleum Reservoir Engineering, vol. 1. Springer-Verlag, Berlin Heidelberg.
Daccord, G., 1987. Chemical dissolution of a porous medium by a reactive fluid. Phys. Rev. Lett. 58 (5), 479–482.
Daccord, G., Lenormand, R., 1987. Fractal patterns from chemical dissolution. Nature 325, 41–43.
Daccord, G., Lenormand, R., Lietard, O., 1993a. Chemical dissolution of a porous medium by a reactive fluid-1. model for the "wormholing" phenomenon. Chem. Eng. Sci. 48 (1), 169–178.
Daccord, G., Lenormand, R., Lietard, O., 1993b. Chemical dissolution of a porous medium by a reactive fluid-2. convection vs. reaction, behavior diagram. Chem. Eng. Sci. 48 (1), 179–186.
Deutsch, C.V., Journel, A.G., 1998. Geostatistical Software Library and User's Guide, second ed. Oxford University Press, New York.
Fredd, C.N., Fogler, H.S., 1998. Influence of transport and reaction on wormhole formation in carbonate porous media. AIChE J. 44 (9), 1933.
Fredd, C.N., Tjia, R., Fogler, H.S., 1997. The existence of an optimum Damkohler number for matrix stimulation of carbonate formations. In: SPE 38167, Presented at SPE European Formation Damage Conference, Hague, The Netherlands, 2–3 June 1997.
Frick, T.P., Mostofizadeh, B., Economides, M.J., 1994. Analysis of radial core experiments for hydrochloric acid interaction with limestones. In: SPE27402, Presented at SPE International Symposium on Formation Damage Control, Lafayette, Louisiana, 7–10 February 1994.
Furui, K., Burton, R.C., Burkhead, D.W., Abdelmalek, N.A., Hill, A.D., Zhu, D., Nozaki, M., 2010. A comprehensive model of high-rate matrix acid stimulation for long horizontal wells in carbonate reservoirs. In: SPE134265, Presented at SPE Annual Technical Conference and Exhibition, Florence, Italy, 19–22 September 2010.
Gdanski, R., 1999. A fundamentally new model of acid wormholing in carbonate. In: SPE54719, Presented at SPE European Formation Damage Conference, Netherlands, 31 May–01 June 1999.
Golfier, F., Zarcone, C., Bazin, B., Lenormand, R., Lasseux, D., Quintard, M., 2002. On the ability of a Darcy-scale model to capture wormhole formation during the dissolution of a porous medium. J. Fluid Mech. 457, 213–254.
Greenkorn, R.A., 1983. Flow Phenomena in Porous Media: Fundamentals and Applications in Petroleum, Water, and Food Production. Marcel Dekker, New York and Basel.
Gupta, N., Balakotaiah, V., 2001. Heat and mass transfer coefficients in catalytic monoliths. Chem. Eng. Sci. 56 (16), 4771–4786.
Hoefner, M.L., Fogler, H.S., 1988. Pore evolution and channel formation during flow and reaction in porous media. AIChE J. 34 (1), 45–54.
Hollis, C., Vahrenkamp, V., Tull, S., Mookerjee, A., Taberner, C., Huang, Y., 2010. Pore system characterisation in heterogeneous carbonates: an alternative approach to widely-used rock-typing methodologies. Mar. Pet. Geol. 27 (4), 772–793.
Huang, T., Hill, A.D., Schechter, R., 1997. Reaction rate and fluid loss: the keys to wormhole initiation and propagation in carbonate acidizing. In: SPE37312, Presented at SPE International Symposium on Oilfield Chemistry, Houston, Texas, 18–21 February 1997.
Huang, T., Zhu, D., Hill, A.D., 1999. Prediction of wormhole population density in carbonate matrix acidizing. In: SPE54723, Presented at SPE European Formation Damage Conference, Hague, 31 May–01 June 1999.
Hung, K.M., Hill, A.D., Sepehrnoori, K., 1989. A mechanistic model of wormhole growth in carbonate matrix acidizing and acid fracturing. J. Pet. Technol. 41 (1), 59–66.
Izgec, O., Keys, R., Zhu, D., Hill, A.D., 2008. An intergrated theoretical and experimental study on the effects of multiscale heterogeneities in matrix acidizing of carbonates. In: SPE115143, Presented at SPE Annual Technical Conference and Exhibition, Denver, Colorado, USA, 21–24 September 2008.
Izgec, O., Zhu, D., Hill, A.D., 2009. Models and methods for understanding of early acid breakthrough observed in acid core-floods of vuggy carbonates. In: SPE122357, Presented at SPE European Formation Damage Conference, Scheveningen, The Netherlands, 27–29 May 2009.
Kalia, N., Balakotaiah, V., 2007. Modeling and analysis of wormhole formation in reactive dissolution of carbonate rocks. Chem. Eng. Sci. 62 (4), 919–928.
Kalia, N., Balakotaian, V., 2009. Effect of medium heterogeneities on reactive dissolution of carbonates. Chem. Eng. Sci. 64 (2), 376–390.

Liu, X., Ormond, A., Bartko, K., Ortoleva, P., 1997. A geochemical reaction-transport simulator for matrix acidizing analysis and design. J. Pet. Sci. Eng. 17 (1-2), 181–197.

Panga, M.K.R., Ziauddin, M., Balakotaiah, V., 2005. Two-scale continuum model for simulation of wormholes in carbonate acidization. AIChE J. 51 (12), 3231–3248.

Schoenfelder, W., Glaser, H., Mitreiter, I., Stallmach, F., 2008. Two-dimensional NMR relaxometry study of pore space characteristics of carbonate rocks from a Permian aquifer. J. Appl. Geophys. 65 (1), 21–29.

Tardy, P.M.J., Lecerf, B., Chrisianti, Y., 2007. An experimentally validated wormhole model for self-diverting and conventional acids in carbonate rocks under radial flow conditions. In: SPE107854, Presented at SPE European Formation Damage Conference, Scheveningen, The Netherlands, 30 May–1 June 2007.

Ziauddin, M., Bize, E., 2007. The effect of pore-scale heterogeneities on carbonate stimulation treatments. In: SPE104627, Presented at SPE Middle East Oil and Gas Show and Conference, Bahrain, Kingdome of Bahrain, 11–14 March 2007.